ACS Catalysis

Research Article

pubs.acs.org/acscatalysis

Platinum-Coated Nickel Nanowires as Oxygen-Reducing Electrocatalysts

Shaun M. Alia,[†] Brian A. Larsen,[†] Svitlana Pylypenko,[‡] David A. Cullen,[§] David R. Diercks,[‡] K.C. Neyerlin,[†] Shyam S. Kocha,[†] and Bryan S. Pivovar*[,†]

[†]Chemical and Materials Science Center, National Renewable Energy Laboratory, Golden, Colorado 80401

[‡]Department of Metallurgical and Materials Engineering, Colorado School of Mines, Golden, Colorado 80401

[§]Materials Science and Technology Division, Oak Ridge National Laboratory, Oak Ridge, Tennessee 37831

Supporting Information

ABSTRACT: Platinum (Pt)-coated nickel (Ni) nanowires (PtNiNWs) are synthesized by the partial spontaneous galvanic displacement of NiNWs, with a diameter of 150−250 nm and a length of 100−200 μm. PtNiNWs are electrochemically characterized for oxygen reduction (ORR) in rotating disk electrode half-cells with an acidic electrolyte and compared to carbon-supported Pt (Pt/HSC) and a polycrystalline Pt electrode. Like other extended surface catalysts, the nanowire morphology yields significant gains in ORR specific activity compared to Pt/HSC. Unlike other extended surface approaches, the resultant materials have yielded exceptionally high surface areas, greater than 90 $m^2\ g_{Pt}^{-1}$. These studies have found that reducing the level of Pt displacement increases Pt surface area and ORR mass activity. PtNiNWs produce a peak mass activity of 917 mA mg_{Pt}^{-1}, 3.0 times greater than Pt/HSC and 2.1 times greater than the U.S. Department of Energy target for proton-exchange membrane fuel cell activity.

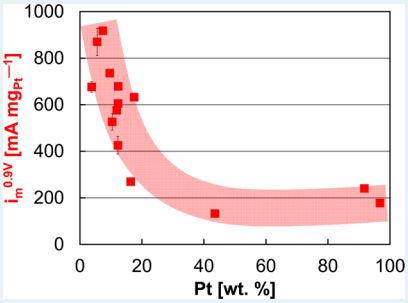

KEYWORDS: *oxygen reduction reaction, fuel cells, electrochemistry, galvanic displacement, electrocatalysis*

INTRODUCTION

Platinum (Pt) nanoparticles supported on high surface area carbon (Pt/HSC) are typically used as proton-exchange membrane fuel cell (PEMFC) catalysts due to a high surface area and moderately high mass activity for the oxygen-reduction reaction (ORR). Although Pt/HSC has reasonable ORR activity, the commercialization of PEMFCs is primarily limited by catalyst cost; a reduction in catalyst cost will allow for the accelerated commercialization of PEMFCs.[1] To meet these cost targets, the U.S. Department of Energy (DOE) set ORR mass activity targets (2017−2020) on a Pt group metal (PGM) basis of 440 mA mg_{PGM}^{-1} for automotive PEMFCs. The durability of Pt/HSC in PEMFCs at low loadings is also a concern.[2] Pt/HSC durability is limited by corrosion of the carbon support and Pt surface area loss by surface-tension-driven aggregation, Ostwald ripening, and potential-driven dissolution.[3,4]

Pt transition metal alloys, particularly in the case of nickel (Ni), have previously been studied for ORR activity.[5] Nørskov et al., Paulus et al., and Stamenkovic et al. studied polycrystalline films of Pt alloyed with transition metals.[6−8] In all three studies, the Pt Ni alloy was found to produce a specific activity greater than double that of polycrystalline Pt (Poly Pt). Stamenkovic also studied low-index Pt Ni facets, finding that Pt_3Ni (111) was 10 times more active for ORR than Pt (111).[9] In nanoscale catalysts, Stamenkovic et al. characterized nanostructured thin films, finding that Pt Ni alloys exceeded the DOE mass activity target.[10] Strasser et al. and others developed Pt Ni polyhedrals, finding a significant ORR benefit in comparison to pure Pt and in cases exceeded the DOE activity target.[11−16] Paulus et al. and Du et al. also studied Pt Ni nanoparticles, finding a significant improvement in the ORR mass activity compared to Pt nanoparticles.[17,18]

Pt nanotubes were previously synthesized, demonstrating improved ORR activity and durability characteristics compared to conventional Pt catalysts.[19] Although a significant improvement was observed in the specific activity of the extended network catalysts, the ORR mass activity was not high enough to meet the DOE target. Subsequent efforts focused on increasing Pt utilization by adding porosity to the nanotubes, studying alternative morphologies, and using palladium and copper substrates to reduce the Pt content.[20−23] Ni nanowires (NiNWs) were used as a template in this study to improve Pt ORR activity by creating an extended surface with the added possibility of a beneficial Ni alloying effect.[24,25] Ni was also examined in this study to avoid template metals that could potentially migrate through the PEMFC membrane and poison the anode catalyst during fuel cell operation (redox potential −0.25 V vs a reversible hydrogen electrode, RHE). This study has benefitted from other related, collaborative work with Yan et al. at the University of Delaware and California-Riverside.[23,26]

Received: November 18, 2013
Revised: January 21, 2014
Published: February 25, 2014

   dx.doi.org/10.1021/cs401081w | *ACS Catal.* 2014, 4, 1114−1119

EXPERIMENTAL SECTION

Pt-coated NiNWs (PtNiNWs) were synthesized by the spontaneous galvanic displacement of NiNWs. At a low Pt content (3.8−16.4 wt % Pt), displacement occurred solely by exposure to potassium tetrachloroplatinate. NiNWs (35 mg as received from PlasmaChem GmbH) were dispersed in 70 mL of water heated to 90 °C under magnetic stirring. Potassium tetrachloroplatinate in 10 mL of water was added dropwise to the NiNW dispersion by syringe pump over a period of 15 min. PtNiNW synthesis proceeded at 90 °C for 2 h. Varying amounts of potassium tetrachloroplatinate (3.1 mg−1.0 g) yielded a variety of Pt displacements (3.8−16.4 wt % Pt, as measured by inductively coupled plasma-mass spectrometry, ICP-MS, Figure S.1). Although an excess of the Pt precursor was provided, potassium tetrachloroplatinate was not able to completely displace the NiNWs. Higher levels of Pt displacement were only achieved by adding hydrochloric acid, presumably due to the presence of a Ni oxide layer and the ability of the added acid to etch this layer, thereby exposing unoxidized Ni. NiNWs (35 mg) were dispersed in 70 mL of water heated to 90 °C under magnetic stirring. Potassium tetrachloroplatinate (41.4 mg) in 10 mL of water containing hydrochloric acid was added dropwise to the NiNW dispersion by syringe pump over a period of 15 min. Varying amounts of hydrochloric acid (3.5 μL−1.3 mL) yielded a variety of Pt displacements (17.5−96.8 wt % Pt, as measured by ICP-MS, Figure S.1). PtNiNW synthesis proceeded at 90 °C for 2 h. All PtNiNW samples were subsequently washed in water and isopropanol.

ICP-MS measurements were taken on a Thermo Scientific iCAP Q. PtNiNWs were digested in aqua regia and diluted to three concentrations that were calibrated to a blank and three standards. Each measurement was taken three times with a dwell time of 0.15 s; standard deviations between these iterations were less than 2%. Catalyst compositions were determined by the Pt-to-Ni ratio, assuming the catalysts contained only Pt and Ni.

A JEOL JSM-7000F field-emission scanning electron microscope (FESEM) equipped with EDAX Genesis energy-dispersive X-ray spectroscopy (EDS) was used to determine the dimensions, morphology, and composition of the NiNWs and PtNiNWs. Micrographs shown in Figure 7 were obtained with a Philips CM200 transmission electron microscope (TEM). For the TEM analysis of PtNiNWs following rotating disk electrode (RDE) break-in and/or RDE durability testing, PtNiNWs were removed from the RDE tip by sonicating the RDE tip in 1 mL of isopropanol to remove and collect samples. X-ray photoelectron spectroscopy (XPS) analysis was performed on a Kratos Nova X-ray photoelectron spectrometer equipped with a monochromatic Al Kα source operated at 300 W. Samples were mounted on a nonconductive tape adhesive. Survey and high-resolution C 1s, O 1s, Ni 2p, and Pt 4f spectra were acquired at 160 and 20 eV, while providing charge compensation using low-energy electrons. Data analysis was performed using CasaXPS software using the default relative sensitivity factor values provided by the XPS manufacturer. A linear background was applied to C 1s, O 1s, and N 1s spectra, and Shirley background was used for Ni 2p and Pt 4f. Quantification is based on analysis of at least three areas per sample.

X-ray diffraction (XRD) measurements were taken on a Bruker D8 Discover using 40 kV and 35 mA in the 2θ range 15°−87° over 6 min. Samples were pipetted and dried onto a glass (silica) slide and encapsulated (capped) by polyvinyl pyrollidone (dispersed in methanol, dried).

TEM samples were also prepared by embedding PtNiNWs in epoxy resin, then cutting ∼50 nm slices using diamond-knife ultramicrotomomy (Figure 3 and Figures S.2−S.5). Because the wires were placed randomly within the epoxy, wires of many different orientations, including cross sections, were available for study. High-resolution scanning transmission electron microscopy (STEM) images and EDS images were recorded in a JEOL JEM 2200FS equipped with a Bruker XFlash SDD detector.

Specimens were prepared for atom probe tomography (APT) analysis using a previously described nanowire lift-out method.[27] APT measurements were made using a Cameca LEAP 4000X Si. The instrument was operated in laser pulsed mode with a laser energy of 80 pJ, a pulse rate of 500 kHz, a base temperature of 50 K, and a detection rate of 5 ions per 1000 pulses.

Electrochemical experiments were conducted in a RDE half-cell, with a glassy carbon working electrode, a Pt mesh counter electrode, and a RHE (Pt wire in a hydrogen-saturated electrolyte) reference electrode.[28,29] Rotation of the working electrode was controlled with a modulated speed rotator (Pine Instrument Company), and electrochemical measurements were taken on a single-channel Autolab potentiostat (Eco Chemie, Metrohm Autolab B.V.).

PtNiNW inks were prepared at a concentration of 0.15−0.20 mg_{PtNi} mL^{-1} for 5 mL (3.8 mL water, 1.2 mL isopropanol). Inks were iced for 5 min prior to adding the Nafion ionomer (4 μL mL^{-1}). PtNiNW inks were sonicated in ice for 30 s (horn), 30 min (bath), 30 s (horn), 10 min (bath), and 30 s (horn) prior to dispensing 10 μL on the glassy carbon working electrode. The electrodes were then dried for 20 min at 40 °C. Ink concentrations were confirmed by weighing dried 100 μL aliquots on a microbalance (three samples, two iterations). Electrode loadings were increased by adding additional ink (in 10 μL increments) with the inks continuously sonicated (20 min bath, 30 s horn) during this process. Inks were then added to graphitized carbon nanofibers (60 wt %), and the electrode preparation process was repeated. Although PtNiNW electrodes were characterized for a wide loading range, electrodes with a 30−40 μg_{PtNi} cm_{elec}^{-2} loading were used in the comparison studies. Pt/HSC (46 wt % Pt, Tanaka Kikinzoku Kogyo) inks were made by dispersing 7.6 mg of catalyst in 10 mL (7.6 mL water, 2.4 mL isopropanol, 40 μL Nafion ionomer). The Pt/HSC ink was sonicated in ice (20 min bath) prior to dispensing (10 μL) on the glassy carbon working electrode.

Catalyst electrochemically active surface areas (ECAs) were determined during cycling voltammograms in an argon-saturated 0.1 M perchloric acid ($HClO_4$) electrolyte from the charge associated with hydrogen adsorption on Pt, assuming a Coulombic charge of 210 μC cm^{-2}.[30] Cyclic voltammograms were performed on PtNiNWs in the range of 0.025−1.4 V versus RHE at 100 mV s^{-1}; cyclic voltammograms were performed on Pt/HSC in the range of 0.025−1.0 V versus RHE at 20 mV s^{-1}. ORR polarization curves were taken during anodic scans (−0.01−1.00 V vs RHE) in an oxygen-saturated 0.1 M $HClO_4$ electrolyte. ORR activities were corrected for internal resistance (typically 18−25 Ω depending on measurement), mass transport (by the Koutecky−Levich equation), and the partial pressure of oxygen (624 mmHg at 5674 ft). At this elevation (5674 ft), the diffusion-limited currents (id) of the ORR polarization curves (4.4−4.8 mA cm_{elec}^{-2} at 1600 rpm) were within the range of theoretically anticipated values. Durability experiments were conducted by potential cycling (30 000 cycles, 0.6−1.0 V vs RHE) at 500 mV s^{-1}. Slower cyclic voltammograms (100 mV s^{-1} for PtNiNWs, 20 mV s^{-1} for Pt/HSC) were periodically taken at a wider range (0.025−1.4 V vs RHE for PtNiNWs, 0.025−1.0 V vs RHE for Pt/HSC) to monitor catalyst ECAs. ORR polarization curves were also taken following durability testing.

RESULTS AND DISCUSSION

PtNiNWs were synthesized by the spontaneous galvanic displacement of NiNWs. PtNiNWs were formed with diameters of 150−250 nm and lengths of 100−200 μm, maintaining the morphology of the as-purchased NiNW template (Figure 1 and Figure S.2).

Nanowires were studied as a function of the level of Pt displacement. Although NiNWs had smooth surfaces, Pt displacement resulted in small surface features with sizes in the 2−4 nm range (Figure S.3). At a low displacement level (9.6 and 12.3 wt % Pt), Pt was constrained to the nanowire surface (Figure S.4). EDS line scans on cross-sectioned PtNiNWs with 9.6 wt % Pt found a Pt surface-layer thickness typically between 10 and 15 nm (Figure 2). Line scans on PtNiNWs (11.9 wt % Pt) from atom probe experiments similarly found a Pt response within the first 10 nm of the

dx.doi.org/10.1021/cs401081w | ACS Catal. 2014, 4, 1114−1119

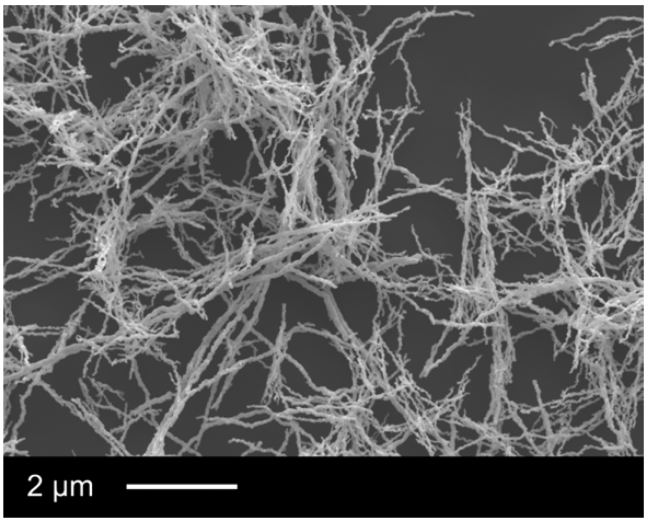

Figure 1. FESEM image of PtNiNWs (7.4 wt % Pt).

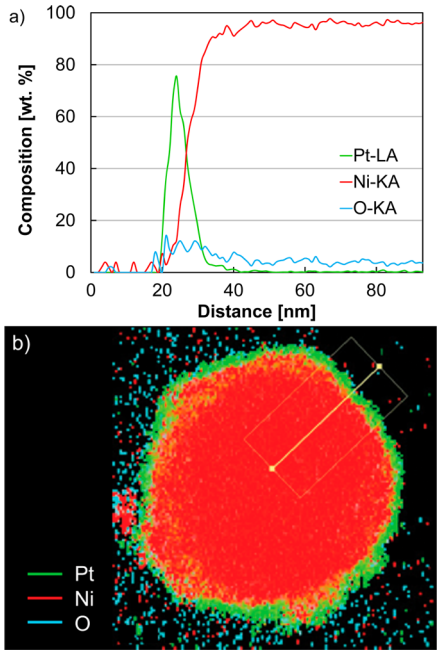

Figure 2. (a) EDS line scan of cross-sectioned PtNiNWs (9.6 wt % Pt) in STEM. (b) EDS map of cross-sectioned PtNiNWs (9.6 wt % Pt) in STEM.

nanowire (Figure 3). Both XPS and STEM found a thin Ni oxide layer, nanometers in scale, on the surface of the NiNWs (Table S.1 and Figure S.2 a, b). The oxide content near the surface persisted in partial Pt galvanic displacements where acid was not added (Table S.1, Figures 2 and 3). At a low Pt content (3.8−16.4 wt % Pt), displacement occurred solely by exposure of the NiNWs to the Pt precursor. Although excess Pt precursor was supplied, greater displacements were not achieved; the thin oxide layer on the NiNWs likely prevented further displacement. Greater levels of Pt displacement (17.5−96.8 wt % Pt) were achieved by adding hydrochloric acid during synthesis. At a high degree of displacement (96.8 wt % Pt), PtNiNWs were found to be hollow with a porous wall thickness of 20−60 nm (Figure S.5).

Cross-sectioned STEM provided information on elemental composition as a function of distance into the PtNiNW. These

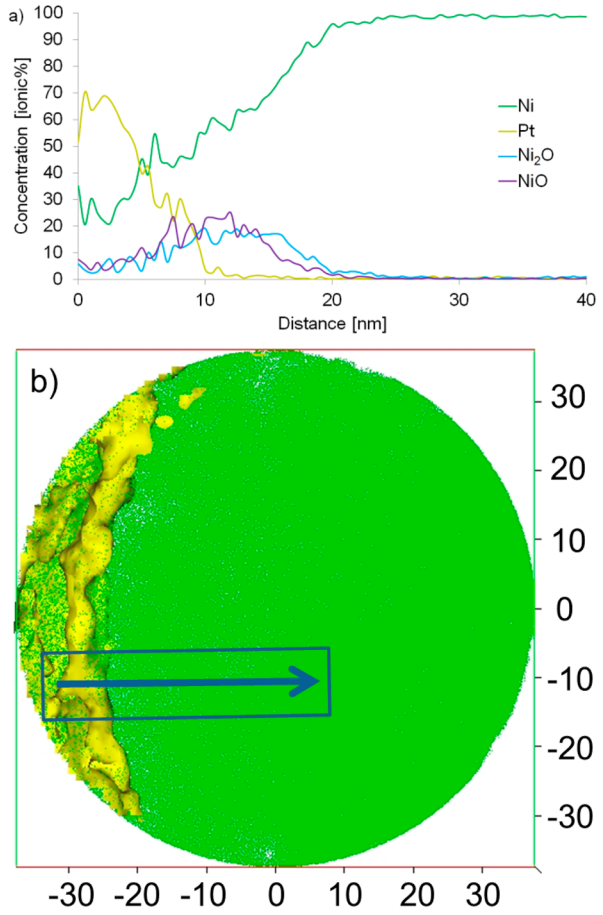

Figure 3. (a) Atom probe line-scan and (b) atom probe reconstruction of a PtNiNW (11.9 wt % Pt) with Pt in yellow and Ni in green. The box indicates the region of the line-scan data in (a).

experiments, however, represent two-dimensional renderings of three-dimensional materials. Cross-sectioned STEM images were taken on microtomed slices of PtNiNWs (and NiNWs) with thicknesses of ∼50 nm (Figure 2, Figure S.2, Figure S.4, and Figure S.5). The PtNiNWs (and NiNWs) were not uniform in shape or diameter over this range; although the EDS map of cross-sectioned PtNiNWs (9.6 wt % Pt) appeared clean, ghosting in these images was possible. For three-dimensional information, atom probe tomography was employed. An atom probe reconstruction shows the outer edge of a PtNiNW and the Ni core (Figure 3b). A 4 nm (z-axis) by 10 nm (y-axis) by 40 nm (x-axis) analysis box from this atom probe reconstruction shows the 1D ionic concentration profile (Figure 3a).

XRD experiments were performed on PtNiNWs. At low Pt displacements, where Ni peaks were clearly visible (9.6 and 12.3 wt % Pt), the Ni lattice was found to be 3.52 Å, matching that of the undisplaced NiNWs. The Pt lattice constants were found to be 3.91 Å ± 0.02 Å (9.6 wt % Pt), 3.90 Å (12.3 wt % Pt), and 3.90 Å ± 0.01 Å (96.8 wt % Pt), slightly compressed compared to the Pt lattice constant (3.92 Å). Further compression of the Pt lattice was not achieved because displacement appeared to yield relatively segregated zones of Pt and Ni (Figure S.3 e,f). It was further anticipated that Pt was not preferentially oriented because the NiNWs appeared to be polycrystalline (Figure S.3 a,b).

dx.doi.org/10.1021/cs401081w | ACS Catal. 2014, 4, 1114−1119

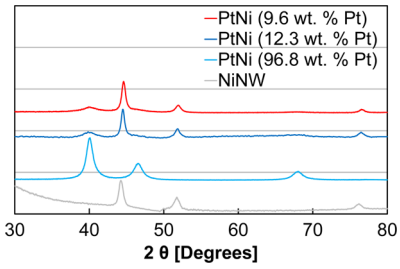

Figure 4. XRD patterns of PtNiNWs (9.6, 12.3, and 96.8 wt % Pt) and NiNWs.

Electrochemical measurements were taken in RDE half-cells. PtNiNWs were dilutely dispersed (0.15−0.2 mg_{PtNi} mL^{-1}) prior to deposition onto a glassy carbon electrode to prevent catalyst aggregation during drying. Multiple aliquots of the catalyst inks were deposited onto the RDE tip to increase the ORR i_d to a level comparable to conventional catalysts (Figure S.6). PtNiNWs were added to the RDE tip with a PtNi loading of 30−40 μg_{PtNi} cm_{elec}^{-2} and were further deposited with and without Nafion ionomer and graphitized carbon nanofibers added to the ink (Figure S.7).[31] The addition of the Nafion ionomer (4 μL mL^{-1}) and carbon (60 wt %) was optimized for ORR mass activity (Figure S.8). Nafion and carbon were found to improve both specific ORR activity and ECA, increasing the mass activity 10−20% and 20−40%, respectively.

PtNiNWs were cleaned prior to electrochemical characterization by potential cycling (10−50 cycles, 0.025−1.4 V vs RHE). This process was needed to provide a relatively stable, Ni-free surface following Pt displacement. Electrochemical testing in a potassium hydroxide (KOH) electrolyte confirmed the presence of Ni on the PtNiNW surface (Figure S.9). Catalyst ECAs were determined during cyclic voltammograms in $HClO_4$ by the charge associated with hydrogen adsorption on t, assuming a Coulombic charge of 210 μC cm^{-2} (Figure 5).[30] The validity of the ECA calculation was confirmed using Poly Pt, which after thorough polishing, was found to have a surface area calculated by charge 1.2 times larger than its geometric surface area (roughness factor of 1.2). The ECA of PtNiNWs dramatically increased with a reduction in the Pt displacement percentage (Figure S.10). Reducing the Pt displacement percentage apparently allowed more of the Pt to remain electrochemically accessible, thereby increasing catalyst ECA on a per Pt basis (Figure S.3 c,d). A peak ECA of 91.3 m^2 g_{Pt}^{-1} was achieved with PtNiNWs 5.6 wt % Pt.

ORR mass and specific activities were determined at 0.9 V vs RHE and corrected for internal resistance, mass transport, and the partial pressure of oxygen (Figure 6). PtNiNWs (7.4 wt % Pt) produced an ORR mass activity of 917 mA mg_{Pt}^{-1}, 3.0 times greater than Pt/HSC (306 mA mg_{Pt}^{-1}) and 2.1 times greater than the DOE activity target in PEMFCs. PtNiNWs produced a wide range of specific ORR activities, from 850 μA cm_{Pt}^{-2} (3.8 wt % Pt) to 2087 μA cm_{Pt}^{-2} (91.7 wt % Pt). The specific activity of PtNiNWs was generally comparable to previous studies of extended surface catalysts for ORR. The peak specific activity of PtNiNWs (2087 μA cm_{Pt}^{-2}) also came within 93% of Poly Pt (2245 μA cm_{Pt}^{-2}) and was 6.9 times greater than Pt/HSC (304 μA cm_{Pt}^{-2}).

The nature of the extended surface (decreased numbers of low-coordinated sites), the electronic tuning of Pt sites through Ni alloying or nanoparticle-based strain effects, and the preferential exposure of surface facets have each been cited as

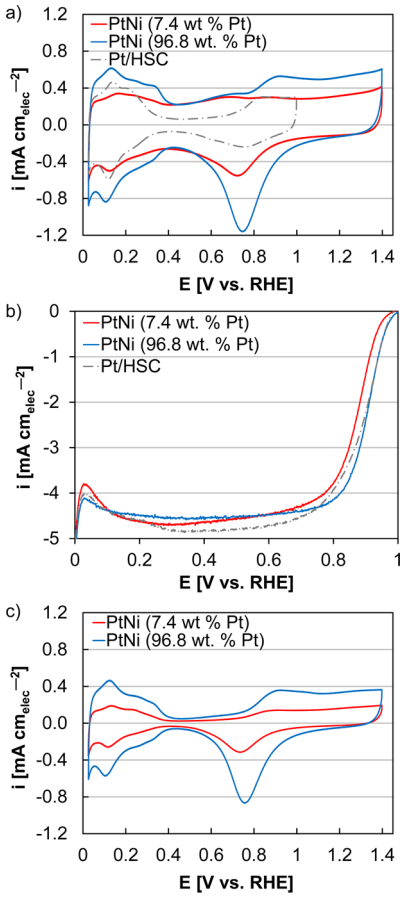

Figure 5. (a) Cyclic voltammograms and (b) ORR polarization curves of PtNiNWs (7.4 and 96.8 wt % Pt, with graphitized carbon nanofibers 60 wt % added to the inks) and Pt/HSC. (c) Cyclic voltammograms of PtNiNWs (7.4 and 96.8 wt % Pt, without graphitized carbon nanofibers). Catalyst loadings on the RDE tip were the following: PtNiNWs (7.4 wt % Pt) 33.7 μg_{PtNi} cm_{elec}^{-2}; PtNiNWs (96.8 wt % Pt) 38.9 μg_{PtNi} cm_{elec}^{-2}; and Pt/HSC 17.8 μg_{Pt} cm_{elec}^{-2}. The ids of the ORR polarization curves are lower than typically found at sea-level due to elevation (5674 ft). Further details on the ORR experiments and activity corrections can be found in the experimental section.

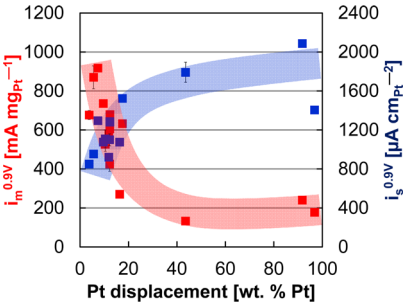

Figure 6. Mass and specific ORR activities of PtNiNWs as a function of percent Pt displacement. The inks used to prepare the RDE tips contained graphitized carbon nanofibers (60 wt %) and a Nafion ionomer (4 μL mL^{-1}). ORR activities were corrected for internal resistance and the partial pressure of oxygen at 0.9 V vs RHE (1600 rpm, 20 mV s^{-1}) in an oxygen-saturated 0.1 M $HClO_4$ electrolyte.

factors for the increased activity of materials similar to those presented here compared to nanoparticles.[6,19,32] During the galvanic displacement of PtNiNWs, Pt is deposited as a thin-film "shell" with porous, nanoparticle-like features. The long-

dx.doi.org/10.1021/cs401081w | ACS Catal. 2014, 4, 1114−1119

range continuity of this Pt "shell" is not well-characterized at this time (particularly at low Pt displacement levels) but nonetheless exhibits relatively high specific activity compared to nanoparticles. The extension of the Pt surface potentially reduces the prevalence of less-active crystal faces or low-coordinated edge sites, and it also avoids carbon to Pt substrate interactions, thereby allowing high specific activity even at high ECA. The presence of Ni within the Pt lattice also potentially electronically tunes Pt by compressing the Pt lattice and impacting the band structure of the surface-exposed Pt, weakening the Pt−O binding strength.[6,33] Pt, however, was found to deposit into relatively segregated zones, reducing the likelihood and/or potential impact of alloying effects. Although the lattice constant was slightly compressed (3.90−3.91 Å compared to 3.92 Å for pure Pt), electronic tuning is not anticipated to be the primary cause for the high specific activity of PtNiNWs. The NiNWs further appeared to be polycrystalline, and high-resolution STEM images of PtNiNWs (9.6 wt % Pt) showed a randomly oriented Pt lattice (Figure S.3 a−d). Because the NiNWs were polycrystalline in nature, it did not appear that displacing Pt aligned into particular growth directions. Also, no particular care was taken in the synthesis of PtNiNWs to expose specific Pt facets; it therefore seemed unlikely that preferentially exposed Pt facets contributed to the high specific activity of PtNiNWs.[32,34] Although there was a degree of scatter in the specific activities of PtNiNWs, the specific activity generally decreased with decreasing Pt displacement (Figure 6). In the higher displaced PtNiNWs (96.8 wt % Pt), Pt deposited into particles with larger feature sizes (Figure S.3 g,h, 5−10 nm) and decreased ECAs. It is possible that the reduction in Pt displacement induced a particle-size effect, although it is relatively modest compared to studies on nanoparticles supported on carbon.[1,24] The Ni content near the PtNiNW surface also increased in the lower displaced samples, introducing the potential for increased alloying effects (Table S.1, 9.6 and 12.2 wt % Pt compared to 96.8 wt % Pt). It was also possible that small amounts of Ni remained on the surface of PtNiNWs at low displacements, inhibiting ORR activity and reducing the specific activity.

Accelerated durability testing was conducted on PtNiNWs and Pt/HSC by potential cycling (30 000 cycles, 0.6−1.0 V vs RHE).[35] Catalyst ECAs were periodically monitored by the charge associated with hydrogen adsorption on Pt (Figure S.11). PtNiNWs with low levels of Pt displacement retained similar ECAs by percentage compared to Pt/HSC. Although extended surface Pt catalysts were previously shown to retain significantly higher ECAs than Pt/HSC under potential cycling, Ni is susceptible to dissolution, potentially reducing durability benefits. EDS measurements of PtNiNWs (9.6 wt % Pt by ICP-MS) as synthesized, following break-in, and following durability testing, however, confirmed a consistent Ni content throughout (Figure 7, 83 wt % Ni by EDS). Fully displaced PtNiNWs (91.7, 96.8 wt % Pt) retained less ECA (by percentage) compared to the partially displaced PtNiNWs and Pt/HSC.

PtNiNWs produced similar ORR specific activities prior to and following potential cycling (Figure 8 and Figure S.12). Although ECA losses were observed, multiple PtNiNW catalysts exceeded the DOE target for PEMFC mass activity following durability testing (7.4, 12.4, and 17.5 wt % Pt). The highest PtNiNW mass activity following potential cycling was 661 mA mg_{Pt}^{-1} (17.5 wt % Pt). In comparison, Pt/HSC produced a mass activity of 225 mA mg_{Pt}^{-1} following 30 000 cycles.

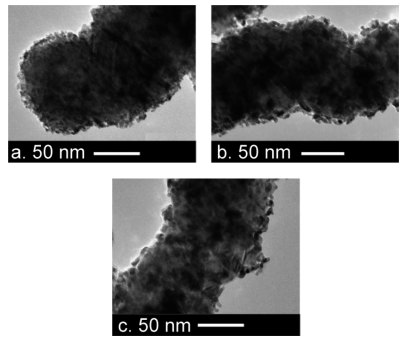

Figure 7. TEM images of PtNiNWs (9.6 wt % Pt) (a) as synthesized, (b) following RDE break-in, and (c) following RDE durability testing (30 000 cycles, 0.6−1.0 V vs RHE).

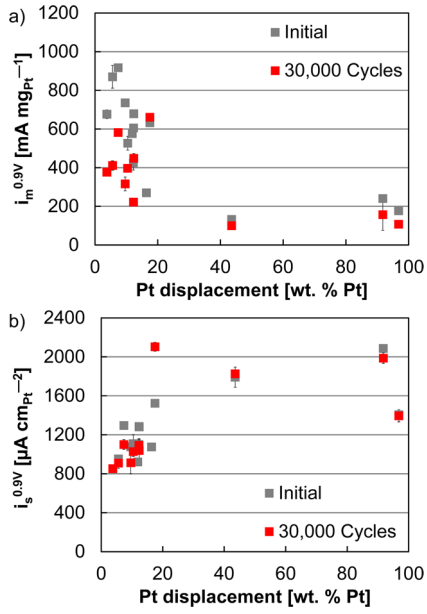

Figure 8. (a) Mass and (b) specific ORR activities of PtNiNWs as a function of percent Pt displacement prior to and following durability testing. The inks used to prepare the RDE tips contained graphitized carbon nanofibers (60 wt %) and a Nafion ionomer (4 μL mL^{-1}). Durability testing was completed by potential cycling (0.6−1.0 V vs RHE) 30 000 times in a nitrogen-saturated 0.1 M $HClO_4$ electrolyte. ORR activities were taken at 0.9 V vs RHE (1600 rpm, 20 mV s^{-1}) in an oxygen-saturated 0.1 M $HClO_4$ electrolyte.

CONCLUSIONS

In summary, PtNiNWs were examined as ORR catalysts in acidic RDE half-cells; PtNiNWs were found to have high activity and durability in electrochemical testing, particularly in catalysts containing less than 20 wt % Pt. As the degree of Pt displacement was reduced, Pt utilization and ECA increased. This ECA improvement at low Pt displacements (less than 20 wt % Pt), reached a value greater than 90 m^2 g_{Pt}^{-1} and allowed for PtNiNWs to produce a maximum ORR mass activity 3.0 times greater than Pt/HSC and 2.1 times greater than the DOE target for PEMFC activity. The samples also showed remarkable durability during potential cycling, maintaining a mass activity of 661 mA mg_{Pt}^{-1} (17.5 wt % Pt) following 30 000 potential cycles. This study demonstrates that PtNiNWs are potentially a much improved ORR catalyst for fuel cells.

dx.doi.org/10.1021/cs401081w | ACS Catal. 2014, 4, 1114−1119

■ ASSOCIATED CONTENT

Supporting Information

Supplementary figures and additional information as noted in the text. This material is available free of charge via the Internet at http://pubs.acs.org.

■ AUTHOR INFORMATION

Corresponding Author

*E-mail: bryan.pivovar@nrel.gov. Fax: (303) 275-3840.

Notes

The authors declare no competing financial interest.

■ ACKNOWLEDGMENTS

Financial support is provided by the U.S. Department of Energy, Office of Energy Efficiency and Renewable Energy, through contract no. DE-AC36-08GO28308 to the National Renewable Energy Laboratory.

■ ABBREVIATIONS

Pt, platinum; Pt/HSC, Pt nanoparticles supported on high surface area carbon; PEMFC, proton-exchange membrane fuel cell; ORR, oxygen reduction reaction; DOE, U.S. Department of Energy; Ni, nickel; Poly Pt, polycrystalline Pt; NiNW, Ni nanowire; RHE, reversible hydrogen electrode; PtNiNW, Pt-coated NiNWs; ICP-MS, inductively coupled plasma-mass spectrometry; FESEM, field-emission scanning electron microscope; EDS, energy-dispersive X-ray spectroscopy; TEM, transmission electron microscope; RDE, rotating disk electrode; XPS, X-ray photoelectron spectroscopy; XRD, X-ray diffraction; STEM, scanning transmission electron microscopy; APT, atom probe tomography; ECA, electrochemically active surface area; $HClO_4$, perchloric acid; i_d, diffusion-limited current; KOH, potassium hydroxide

■ REFERENCES

(1) Gasteiger, H.; Kocha, S.; Sompalli, B.; Wagner, F. *Appl. Catal., B* **2005**, *56*, 9−35.

(2) Ferreira, P.; la O', G.; Shao-Horn, Y.; Morgan, D.; Makharia, R.; Kocha, S.; Gasteiger, H. *J. Electrochem. Soc.* **2005**, *152*, A2256−A2271.

(3) Darling, R.; Meyers, J. *J. Electrochem. Soc.* **2003**, *150*, A1523−A1527.

(4) Borup, R.; Meyers, J.; Pivovar, B.; Kim, Y.; Mukundan, R.; Garland, N.; Myers, D.; Wilson, M.; Garzon, F.; Wood, D.; Zelenay, P.; More, K.; Stroh, K.; Zawodzinski, T.; Boncella, J.; McGrath, J.; Inaba, M.; Miyatake, K.; Hori, M.; Ota, K.; Ogumi, Z.; Miyata, S.; Nishikata, A.; Siroma, Z.; Uchimoto, Y.; Yasuda, K.; Kimijima, K.; Iwashita, N. *Chem. Rev.* **2007**, *107*, 3904−3951.

(5) Marković, N.; Schmidt, T.; Stamenković, V.; Ross, P. *Fuel Cells* **2001**, *1*, 105−116.

(6) Stamenkovic, V.; Mun, B.; Mayrhofer, K.; Ross, P.; Markovic, N.; Rossmeisl, J.; Greeley, J.; Nørskov, J. *Angew. Chem.* **2006**, *118*, 2963−2967.

(7) Stamenković, V.; Schmidt, T.; Ross, P.; Marković, N. *J. Phys. Chem. B* **2002**, *106*, 11970−11979.

(8) Paulus, U.; Wokaun, A.; Scherer, G.; Schmidt, T.; Stamenkovic, V.; Markovic, N.; Ross, P. *Electrochim. Acta* **2002**, *47*, 3787−3798.

(9) Stamenkovic, V.; Fowler, B.; Mun, B.; Wang, G.; Ross, P.; Lucas, C.; Marković, N. *Science* **2007**, *315*, 493−497.

(10) van der Vliet, D.; Wang, C.; Debe, M.; Atanasoski, R.; Markovic, N.; Stamenkovic, V. *Electrochim. Acta* **2011**, *56*, 8695−8699.

(11) Cui, C.; Gan, L.; Li, H.; Yu, S.; Heggen, M.; Strasser, P. *Nano Lett.* **2012**, *12*, 5885−5889.

(12) Cui, C.; Gan, L.; Heggen, M.; Rudi, S.; Strasser, P. *Nat. Mater.* **2013**, *12*, 765−771.

(13) Cui, C.; Ahmadi, M.; Behafarid, F.; Gan, L.; Neumann, M.; Heggen, M.; Cuenya, B.; Strasser, P. *Faraday Discuss.* **2013**, *162*, 91−112.

(14) Wu, J.; Zhang, J.; Peng, Z.; Yang, S.; Wagner, F.; Yang, H. *J. Am. Chem. Soc.* **2010**, *132*, 4984−4985.

(15) Zhang, J.; Yang, H.; Fang, J.; Zou, S. *Nano Lett.* **2010**, *10*, 638−644.

(16) Ahmadi, M.; Behafarid, F.; Cui, C.; Strasser, P.; Cuenya, B. *ACS Nano* **2013**, *7*, 9195−9204.

(17) Du, S.; Lu, Y.; Malladi, S.; Xu, Q.; Steinberger-Wilckens, R. *J. Mater. Chem. A* **2014**, *2*, 692−698.

(18) Paulus, U.; Wokaun, A.; Scherer, G.; Schmidt, T.; Stamenkovic, V.; Radmilovic, V.; Markovic, N.; Ross, P. *J. Phys. Chem. B* **2002**, *106*, 4181−4191.

(19) Chen, Z.; Waje, M.; Li, W.; Yan, Y. *Angew. Chem., Int. Ed.* **2007**, *46*, 4060−4063.

(20) Alia, S.; Zhang, G.; Kisailus, D.; Li, D.; Gu, S.; Jensen, K.; Yan, Y. *Adv. Funct. Mater.* **2010**, *20*, 3742−3746.

(21) Larsen, B.; Neyerlin, K.; Bult, J.; Bochert, C.; Blackburn, J.; Kocha, S.; Pivovar, B. *J. Electrochem. Soc.* **2012**, *159*, F622−F627.

(22) Alia, S.; Jensen, K.; Pivovar, B.; Yan, Y. *ACS Catal.* **2012**, *2*, 858−863.

(23) Alia, S.; Jensen, K.; Contreras, C.; Garzon, F.; Pivovar, B.; Yan, Y. *ACS Catal.* **2013**, *3*, 358−362.

(24) Kinoshita, K. *J. Electrochem. Soc.* **1990**, *137*, 845−848.

(25) Greeley, J.; Stephens, I.; Bondarenko, A.; Johansson, T.; Hansen, H.; Jaramillo, T.; Rossmeisl, J.; Chorkendorff, I.; Nørskov, J. *Nat. Chem.* **2009**, *1*, 552−556.

(26) Pivovar, B.. 2013 DOE Hydrogen and Fuel Cells Program Review. National Renewal Energy Laboratory, U.S. Department of Energy, May 16, 2013. http://www.hydrogen.energy.gov/pdfs/review13/fc007_pivovar_2013_o.pdf.

(27) Diercks, D.; Gorman, B.; Cheung, C.; Wang, G. *Microsc. Microanal.* **2009**, *15*, 254−255.

(28) Takahashi, I.; Kocha, S. *J. Power Sources* **2010**, *195*, 6312−6322.

(29) Garsany, Y.; Baturina, O.; Swider-Lyons, K.; Kocha, S. *Anal. Chem.* **2010**, *82*, 6321−6328.

(30) Biegler, T.; Rand, D.; Woods, R. *J. Electroanal. Chem. Interfacial Electrochem.* **1971**, *29*, 269−277.

(31) Kocha, S.; Zack, J.; Alia, S.; Neyerlin, K.; Pivovar, B. *ECS Trans.* **2013**, *50*, 1475−1485.

(32) Marković, N.; Adžić, R.; Cahan, B.; Yeager, E. *J. Electroanal. Chem.* **1994**, *377*, 249−259.

(33) Nørskov, J.; Rossmeisl, J.; Logadottir, A.; Lindqvist, L.; Kitchin, J.; Bligaard, T.; Jónsson, H. *J. Phys. Chem. B* **2004**, *108*, 17886−17892.

(34) Markovic, N.; Gasteiger, H.; Ross, P. *J. Phys. Chem.* **1995**, *99*, 3411−3415.

(35) Kocha, S. In *Polymer Electrolyte Fuel Cell Degradation*; Mench, M. Kumbur, E. C., Veziroglu, T.N., Eds.; 2011; pp 89−185.